Available online at www.sciencedirect.com
ScienceDirect
Acta Materialia 58 (2010) 5759–5767
Acta MATERIALIA
www.elsevier.com/locate/actamat

# Experimental and finite-element analysis of the anisotropic response of high-purity α-titanium in bending

Michael E. Nixon [a], Ricardo A. Lebensohn [b], Oana Cazacu [c,*], Cheng Liu [b]

[a] Air Force Research Laboratory, Munitions Directorate, Eglin AFB, FL 32542, USA
[b] Los Alamos National Laboratory, MST Division, Los Alamos, NM 87545, USA
[c] Department of Mechanical and Aerospace Engineering, University of Florida, REEF, 1350 N Poquito Road, Shalimar, FL 32539, USA

Received 19 March 2010; received in revised form 18 June 2010; accepted 20 June 2010
Available online 17 July 2010

**Abstract**

In this paper, we present results of four-point bending tests performed on beams of high-purity α-titanium material. These tests have been performed at room temperature for different beam configurations and loading orientations with respect to the orthotropy axes of the material. Digital image correlation was used to determine local strains in the deformed beams. Experimental results compare very well with the predictions of finite-element simulations obtained using the elastic/plastic model developed by Nixon et al. (2010) [12]. Specifically, we compare local deformations and the cross-sections of each beam for all loading configurations. We show that the model predicts with great accuracy the tension–compression asymmetry and the evolving anisotropy of the material. The experimentally observed upward shift of the neutral axis, as well as the rigidity of the response along the hard to deform *c*-axes are very well described by the proposed model.


*Keywords:* Twinning; α-Titanium; Bent beams; Orthotropy; Elastoplastic model

## 1. Introduction

Pure titanium has a hexagonal close-packed (hcp) structure with a *c*/*a* ratio of 1.587, i.e. lower than the ideal *c*/*a* ratio of 1.633. There are three principal types of titanium alloys: α or near α alloys, α–β alloys and β alloys. Titanium alloys in the low- and medium-temperature regime mainly consist of the hcp α-phase with very little dispersed β phase in between the α grains. These hcp-dominated metals are known to display plastic anisotropy and a strong tension–compression asymmetry. Considerable efforts have been devoted to the understanding of the specific plastic deformation mechanisms at room temperature in pure titanium (e.g. [14,11]) and in commercial-purity titanium [3]. Two types of deformation modes, slip and twinning, occur in titanium and its alloys during plastic deformation at room temperature. It is generally agreed that pronounced yield asymmetry is associated with the activation of twinning. Previous studies (e.g. [7,10,9]) have also shown that classic plasticity models, such as $J_2$ plasticity or [4], are unable to capture this asymmetry, which results from the combination of a sharp initial basal texture and the polarity of deformation twinning. Twinning plays two important roles in α-titanium. It is a main contributor to texture evolution by reorienting the twinned areas [3]. Furthermore, twinning drastically influences the strain-hardening behavior (e.g. [14]). Accurate and realistic modeling of the behavior of α-titanium thus requires incorporation of the effects of twinning on the mechanical response. In Ref. [12] an experimental investigation on the quasi-static, room temperature, tensile and compressive response of a high-purity α-titanium was reported. It was shown that the hardening rate of this material is strongly dependent on the loading

* Corresponding author.
*E-mail addresses:* nixon@eglin.af.mil (M.E. Nixon), lebenso@lanl.gov (R.A. Lebensohn), cazacu@reef.ufl.edu (O. Cazacu).

1359-6454/$36.00 © 2010 Acta Materialia Inc. Published by Elsevier Ltd. All rights reserved.
doi:10.1016/j.actamat.2010.06.051

direction and the sense of the applied load. An elastoplastic model that accounts for the observed anisotropy and tension–compression asymmetry was also developed. The ability of the proposed model to capture the main features of the observed behavior were assessed by comparing the experimental data with simulation results in terms of stress–strain response in uniaxial tensile and compression tests.

In this paper, we report the results of a series of four-point bend experiments performed on specimens cut from the same α-titanium plate (Section 2). To quantify the directionality of the tension-compression asymmetry of the material, tests were conducted on beam specimens with the long axis aligned along different directions of symmetry of the plate and for several loading directions. A benefit associated with conducting bending tests is that one can produce a continuous gradient of strain, from compressive in the upper fibers to tensile in the bottom fibers (by fiber we mean a thin volume of material, parallel to the longitudinal axis, which can be considered to be stretched or compressed homogeneously) of the beam. Such data may be further used to test constitutive models, specifically the accuracy in modeling twinning effects on deformation (e.g. [6,8]). Specifically, in this work we apply the macroscopic model of Ref. [12] to simulate the three-dimensional deformation of the α-titanium beams. An overview of this model, along with the identification procedures for determination of the model parameters, are presented in Section 3. Local strain measurements determined using digital image correlation (DIC) techniques as well as measured final cross-sections are compared with the finite-element simulations based on this model (Section 4).

## 2. Four-point bending tests

The material used in this work was high-purity (99.999%) titanium purchased from Alpha Aesar of Johnson Matthey Electronics, Inc., (Spokane, WA). The material was supplied in the form of a 15.87 mm thick cross-rolled disk of 254 mm diameter. Optical microscopy showed that the as-received material has equiaxed grains with an average grain size of about 20 μm. It exhibits orthotropic texture resulting from the rolling process (see [12]). Comparison between compressive and tensile stress–strain response along the rolling direction is presented in Fig. 1. Although, initially there is no significant difference in yielding behavior (at 0.02% strain offset, the yield stress is 175 MPa), a very pronounced tension–compression asymmetry is observed after about 10% strain. Note the especially sharp difference in hardening evolution. While in tension, the material hardens gradually until plastic localization (necking) occurs at about 30% strain, in compression strain-hardening is strongly non-linear, with a very pronounced increase in hardening rate observed at about 10% strain. This change in hardening may be indicative of twinning. This hypothesis was verified by the analysis of the textures of the deformed specimen (see Ref. [12] for details).

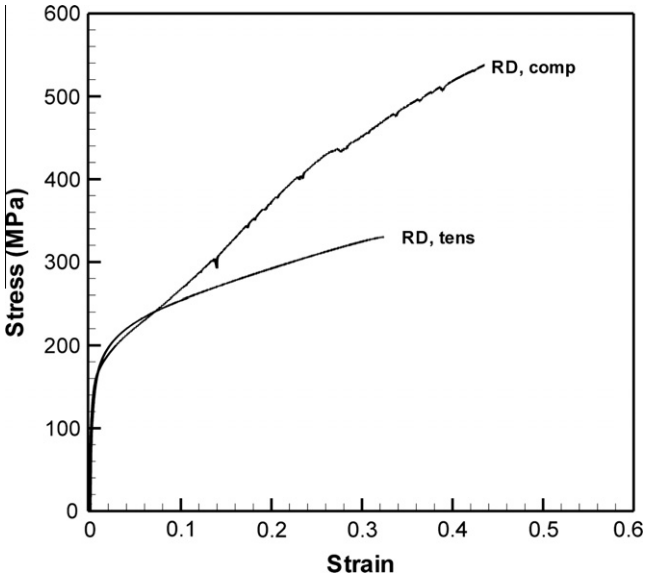


Fig. 1. Comparison between the compression and tension response in the rolling direction.

Quasi-static uniaxial tensile and compression tests on specimens cut along different directions of the plate have revealed that the tension–compression asymmetry of this material is highly directional (see Figs. 2 and 3).

To further characterize this tension–compression asymmetry for bending loading, it is necessary to conduct tests for different beam configurations and loading orientations with respect to the orthotropy axes. To this end, four beam samples were cut. Two samples were machined such that the long axis was along the rolling direction while the other

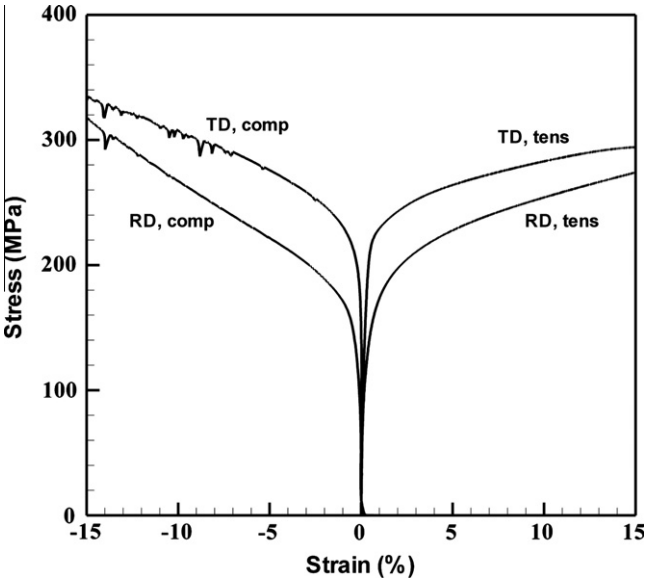


Fig. 2. Comparison between stress–strain response in tension and compression and experimental data for rolling (RD) and transverse (TD) directions, respectively.

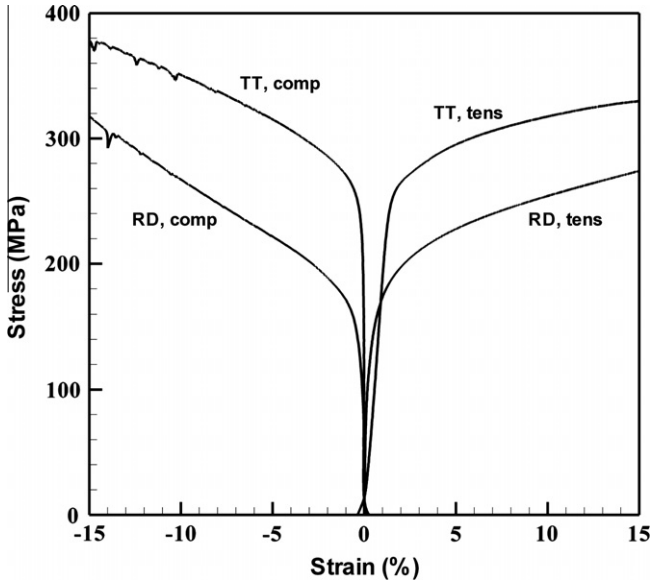


Fig. 3. Comparison between stress–strain response in tension and compression and experimental data for rolling (RD) and through-thickness (TT) directions, respectively.

two samples were machined with the long axis along the transverse direction. For each of these two sets of specimens, one beam was loaded in the through-thickness (TT) direction while the other sample was loaded in the in-plane direction normal to the beam axis. These four test configurations are shown in Fig. 4. To simplify the notations when describing the beam test results, we denote by $(x,y,z)$ the reference frame associated with the orthotropic axes, with $x$ designating the rolling direction, $y$ the transverse direction and $z$ the through-thickness direction.

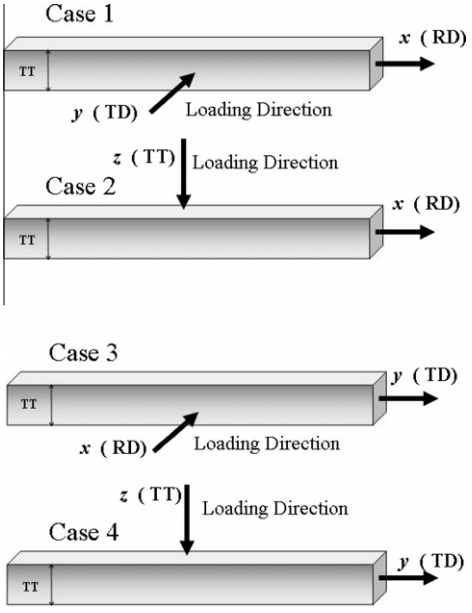


Fig. 4. Four-point bending test specimens: in cases 1 and 2 the long axis of the beam is aligned with the rolling direction ($x$ = RD); for cases 3 and 4 the long axis of the beam is aligned with the transverse direction ($y$ = TD). TT designates the through-thickness direction.

The testing jig with a test specimen is shown in Fig. 5. The two upper pins were moved downwards approximately 5.5 mm, in displacement-controlled mode. Along one side of each beam, a speckle pattern was sprayed and DIC [16] was used to determine the strain field after deformation. The image taken had 88 pixels along the short direction of the beam. The beam dimension in that direction is 6.35 mm. Thus, the physical distance between pixels is 72 μm/pixel. The DIC method can detect displacements of 0.01 pixel; therefore the error is less than 1 μm. A typical undeformed and deformed grid are shown in Fig. 6. Note that the data from the experiment does not cover the entire specimen lateral surface. This is because cells of a grid that covers the gauge area over which the correlation is carried out have a finite size, and the deformation information is given at the center of each cell. All these cells have to be within the specimen surface, and therefore the experimental data points cannot reach the specimen edge.

In addition, the deformed specimens were cut at the midpoint along their axis to examine the final deformed cross-section, and measurements of this cross-section were taken for comparison to the FE simulation results. A contour plot of the experimental axial strain field for each of the loading scenarios (see Fig. 4) are shown in Figs. 7–10. The axial strain is defined as the strain in the long axis

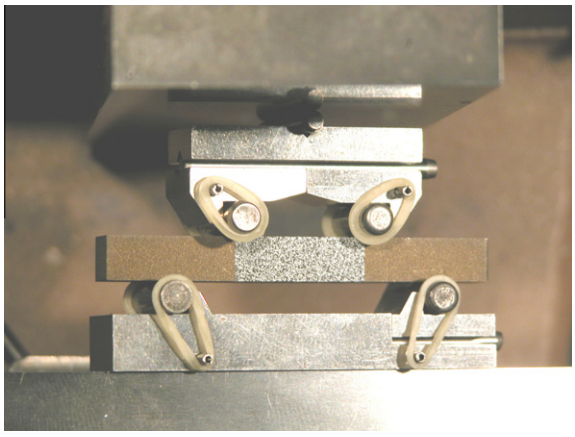

Fig. 5. Four-point beam test jig with test specimen.

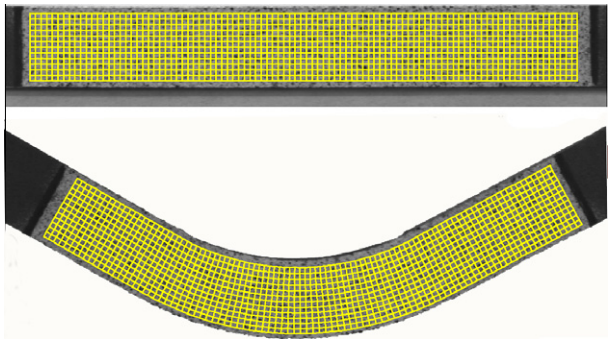

Fig. 6. Typical undeformed and deformed grid used by the DIC technique to generate the experimental strain field.

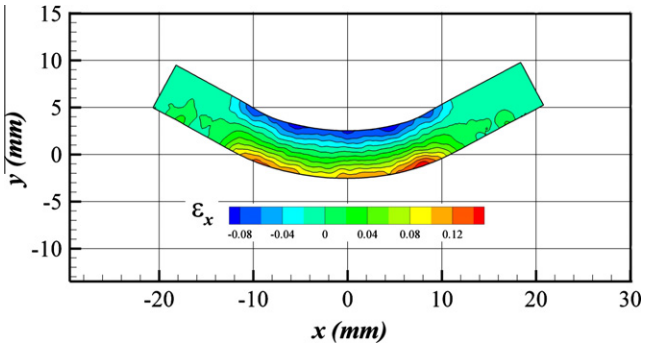


Fig. 7. Experimental axial strain ($\varepsilon_x$) fields for case 1 configuration: long axis in $x$ = RD, loading in $y$ = TD.

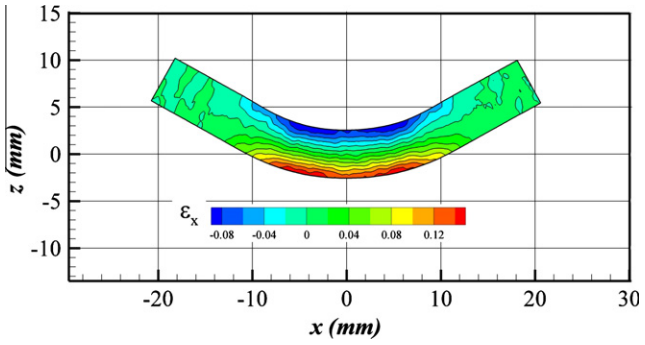


Fig. 8. Experimental axial strain ($\varepsilon_x$) fields for case 2 configuration: long axis in $x$ = RD, loading in $z$ = TT.

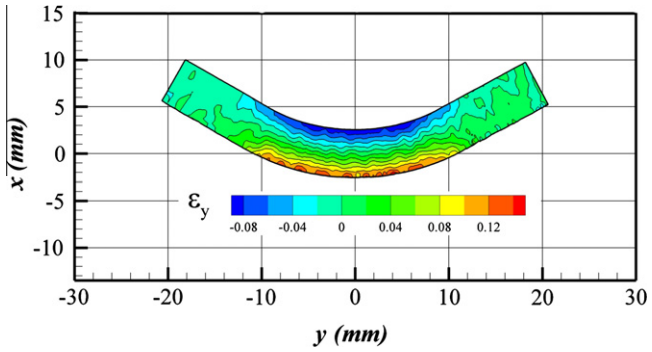


Fig. 9. Experimental axial strain ($\varepsilon_y$) fields for case 3 configuration: long axis in $y$ = TD, loading in $x$ = RD.

direction of the specimen. For cases 1 and 2 loadings, the long axis is along the rolling direction $x$ so the axial strain component is $\varepsilon_x$ while for cases 3 and 4, the long axis corresponds to the transverse direction $y$, therefore the axial strain is $\varepsilon_y$. In all tests, some non-uniform deformation occurred in the direction normal to the plane for which the data were reported, thus introducing a slight error in the computation of the axial strains using the DIC methodology.

In all cases, an upward shift of the neutral axis was observed (i.e. the point at which the longitudinal strain

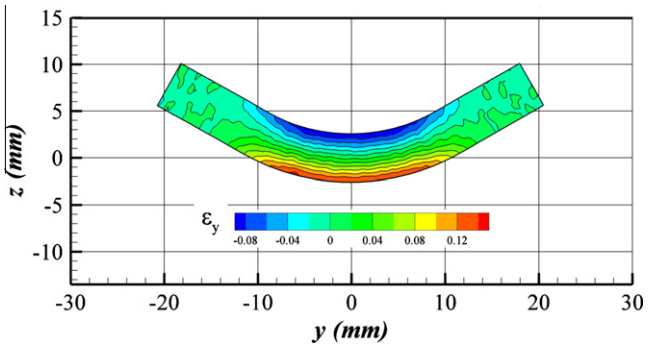


Fig. 10. Experimental axial strain ($\varepsilon_y$) fields for case 4 configuration: long axis in $y$ = TD, loading in $z$ = TT.

vanishes is above the beam's midpoint in the vertical direction). The reason for this shift is related with the different response in tension (softer) and in compression (harder) of the fibers. For example, in the hypothetical extreme case of a material being infinitely hard to deform plastically in compression along the beam's longitudinal direction, the neutral axis would be at the top the sample.

## 3. Elastoplastic constitutive model

Based on quasi-static experimental data in tension and compression, Nixon et al. [12] developed an orthotropic full three-dimensional elastoplastic model. A brief overview of this model is given in the following; a detailed description can be found in Ref. [12]. The onset of plastic deformation is described by a criterion of the form:

$$f\left(J_2^o, J_3^o\right) = \left(J_2^o\right)^{3/2} - c(J_3^o), \tag{1}$$

where $c$ is a material parameter, $J_2^o = (1/2)tr(\mathbf{\Sigma}^2)$ and $J_3^o = (1/3)tr(\mathbf{\Sigma}^3)$ denote the second and third invariant of the transformed stress tensor:

$$\mathbf{\Sigma} = \mathbf{L}[\sigma] \tag{2}$$

$\mathbf{L}$ is a 4th order symmetric tensor ($L_{ijkl} = L_{jikl} = L_{jilk} = L_{klij}$ with $i, j, k, l = 1, 2, 3$) that satisfies (a) the requirement of invariance with respect to the symmetry group of the material, and (b) $L_{1k} + L_{2k} + L_{3k} = 0$ for $k = 1, 2, 3$. This ensures that $\mathbf{\Sigma}$ is traceless, and consequently yielding is insensitive to hydrostatic pressure. With respect to the axes of orthotropy and using Voigt notations, $\mathbf{L}$ is represented by:

$$\mathbf{L} = \begin{bmatrix} \frac{(a_2+a_3)}{3} & -\frac{a_3}{3} & -\frac{a_2}{3} & 0 & 0 & 0 \\ -\frac{a_3}{3} & \frac{(a_1+a_3)}{3} & -\frac{a_1}{3} & 0 & 0 & 0 \\ -\frac{a_2}{3} & -\frac{a_1}{3} & \frac{(a_1+a_2)}{3} & 0 & 0 & 0 \\ 0 & 0 & 0 & a_4 & 0 & 0 \\ 0 & 0 & 0 & 0 & a_5 & 0 \\ 0 & 0 & 0 & 0 & 0 & a_6 \end{bmatrix}. \tag{3}$$

Thus, for three-dimensional stress conditions the orthotropic criterion involves: six anisotropy coefficients (i.e. the independent components of $\mathbf{L}$) and a strength differential

coefficient, $c$. Determination of the material parameters can be done using the measured tensile and compressive flow stresses along different orientations of the plate. The anisotropic criterion (1) reduces to the isotropic criterion of Ref. [2] when $\mathbf{L}$ is equal to the fourth-order deviatoric identity tensor. The equivalent stress, $\bar{\sigma}$, associated with the anisotropic criterion (1) is:

$$\bar{\sigma} = A_1\left[\left(J_2^{\circ}\right)^{3/2} - cJ_3^{\circ}\right]^{1/3}, \tag{4}$$

with

$$A_1 = 3\left[\left(a_2^2 + a_3^2 + a_2a_3\right)^{3/2} - c(a_2 + a_3)a_2a_3\right]^{-1/3}. \tag{5}$$

The hardening variable was considered to be the effective plastic strain $\bar{\varepsilon}_p$ , associated with the effective stress $\bar{\sigma}$ using the work-equivalence principle. Yielding is described as:

$$F(\boldsymbol{\sigma}, \bar{\varepsilon}_p) = \bar{\sigma}(\boldsymbol{\sigma}, \bar{\varepsilon}_p) - Y(\bar{\varepsilon}_p), \tag{6}$$

where $\bar{\sigma}$ is given by (4), while $Y(\bar{\varepsilon}_p)$ is a reference hardening curve (e.g. corresponding to the rolling direction). An associated flow rule is considered, i.e.

$$\dot{\varepsilon}_p = \dot{\lambda}\frac{\partial \bar{\sigma}}{\partial \boldsymbol{\sigma}}, \tag{7}$$

where $\dot{\lambda}$ is the plastic multiplier. In the above equations all stresses and strains are expressed in a materially embedded coordinate system such as to ensure that the resulting incremental constitutive law is objective as described in Ref. [5,15]. To account for the evolution of anisotropy associated with deformation twinning, the interpolation-based methodology proposed in Ref. [13] was used. Thus, using the experimental yield stress data, the anisotropy coefficients corresponding to initial yielding and several values of the equivalent plastic strain are: $\bar{\varepsilon}_p^1 < \bar{\varepsilon}_p^2 < \cdots < \bar{\varepsilon}_p^m$. Next, the effective stress $\tilde{\sigma}^j = \tilde{\sigma}\left\{\boldsymbol{\sigma}, c\left(\bar{\varepsilon}_p^j\right), a_i\left(\bar{\varepsilon}_p^j\right)\right\}$ according to the criterion (4) as well as $Y^j = Y\left(\bar{\varepsilon}_p^j\right)$ corresponding to the each of the individual strain levels $\bar{\varepsilon}_p^j$, $j = 1, \ldots, m$, were calculated. To obtain the yield surface corresponding to any given level of accumulated strain, $\bar{\varepsilon}_p^j < \bar{\varepsilon} < \bar{\varepsilon}_p^{j+1}$ an interpolation procedure was used. Specifically, for the given level $\bar{\varepsilon}_p$, the anisotropic yield function is of the form:

$$F(\boldsymbol{\sigma}, \bar{\varepsilon}_p) = \Gamma(\boldsymbol{\sigma}, \bar{\varepsilon}_p) - \Pi(\bar{\varepsilon}_p), \tag{8}$$

with

$$\Gamma = \xi(\bar{\varepsilon}_p)\cdot\tilde{\sigma}^j + (1 - \xi(\bar{\varepsilon}_p))\cdot\tilde{\sigma}^{j+1}, \tag{9}$$

and

$$\Pi = \xi(\bar{\varepsilon}_p)\cdot Y^j + (1 - \xi(\bar{\varepsilon}_p))\cdot Y^{j+1}. \tag{10}$$

If a linear interpolation scheme is considered, the weighting parameter appearing in Eqs. (8) and (9) is defined as:

$$\xi(\bar{\varepsilon}_p) = \frac{\bar{\varepsilon}_p^{j+1} - \bar{\varepsilon}_p}{\bar{\varepsilon}_p^{j+1} - \bar{\varepsilon}_p^{j}}, \tag{11}$$

such that $\xi(\bar{\varepsilon}_p^j) = 1$ and $\xi(\bar{\varepsilon}_p^{j+1}) = 0$. In this manner, the observed distortion and change in shape of the yield loci could be captured. Obviously, if these coefficients are taken constant, the proposed hardening law reduces to the classic isotropic hardening law. The details of the FE implementation of the model are given in Ref. [12].

## 4. Comparison with FE simulations and discussions

For each of the four bending experiments, the data were compared to FE simulation using the anisotropic elasto-plastic model presented in Section 3. In the interpolation procedure, the anisotropy coefficients corresponding to initial yielding and four other individual prestrain values (up to 20% strain) were considered. The numerical values of these coefficients for each level of prestrain are given in Table 1 while a comparison between the theoretical yield surfaces and experimental values is shown in Fig. 11. Concerning the specific expression of $Y(\bar{\varepsilon}_p)$ in Eq. (6), a Voce-type law was used where $\bar{\varepsilon}_p$ represents the equivalent plastic strain.

Table 1
Yield function (4) coefficients for high-purity α-titanium corresponding to fixed values of the equivalent plastic strain $\bar{\varepsilon}_p$. Note $a_1$ is set to 1 for all cases.

| $\bar{\varepsilon}_p$ | $a_2$ | $a_3$ | $a_4$ | c |
|---|---|---|---|---|
| 0.000 | 0.9186 | 1.9985 | 1.3286 | −0.3975 |
| 0.025 | 0.9071 | 1.7270 | 1.3972 | −0.4202 |
| 0.050 | 0.8343 | 1.6477 | 1.3651 | −0.3422 |
| 0.075 | 0.8576 | 1.6193 | 1.4135 | −0.3746 |
| 0.100 | 0.8902 | 1.6062 | 1.4490 | −0.5142 |
| 0.200 | 0.9443 | 1.4246 | 1.4262 | −9.6852 |

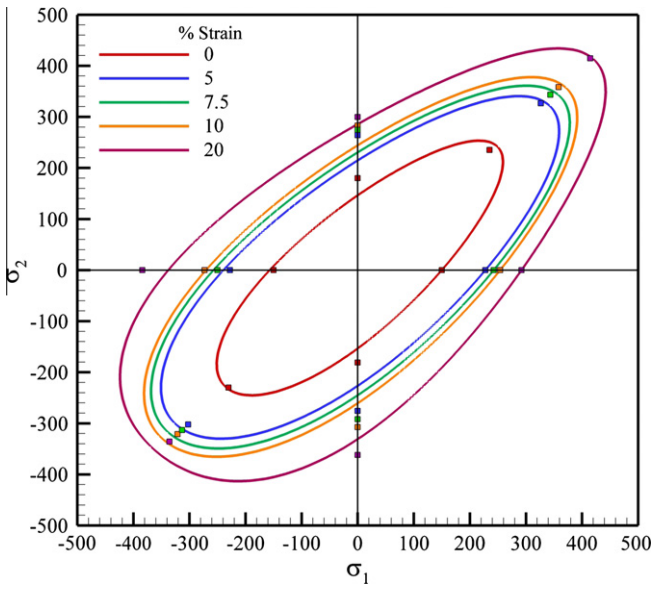


Fig. 11. Theoretical yield surfaces according to (4) and experimental data (symbols) corresponding to fixed values of the equivalent plastic strain $\bar{\varepsilon}_p$. Stresses are in MPa.

The simulated final cross-sections for the four configurations are shown in Fig. 12. As expected, when the hard direction (through thickness) is perpendicular to the loading direction (cases 1 and 3), cross-sections of the beams retain an almost square shape because they do not deform along the $z$ axis. Cases 2 and 4 are similar to each other: the samples develop wedge-shape cross-sections, with more lateral strain in case 4 than in case 2. This is consistent with the material being harder in the transverse direction than in the rolling direction as shown in the uniaxial tests. This can be seen in Fig. 3, which shows that, for strain levels below 15%, the material's yield strength in the transverse direction is higher than that in the rolling direction for both tensile and compressive loadings.

In what follows, comparisons between FE axial strains obtained with the proposed anisotropic model and experimental axial strains obtained by DIC are presented. For case 1 loading (see Fig. 4), comparison of the respective strain contours is shown in Fig. 13a, while Fig. 13b shows a comparison of the axial strain vs. height of the beam variation at the center of the beam. Note again that the data from the experiment does not cover the entire area, due to the DIC technique used. A very good agreement between the experiment and simulation is observed. In particular, the upward shift of the neutral axis of the beam is very well captured by the model. In the model the anisotropy coefficients $a_i$ and the strength differential parameter $c$ are functions of the accumulated plastic strain. These results show that the model developed captures accurately the tension–compression asymmetry and its evolution. To further validate the model, the deformed beams were sectioned at the midpoint and the photographed sections were

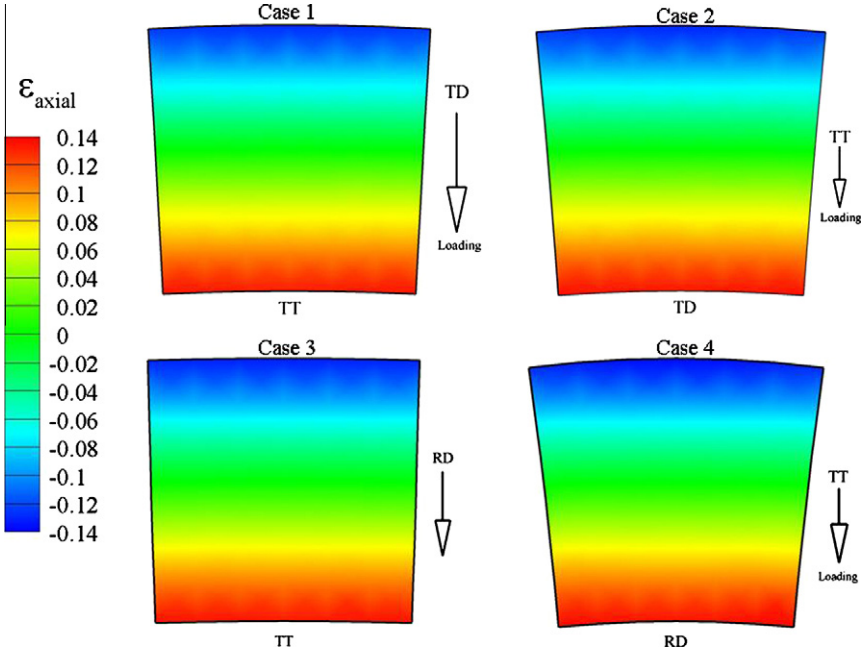


Fig. 12. Simulated final cross-sections for the four beam configurations.

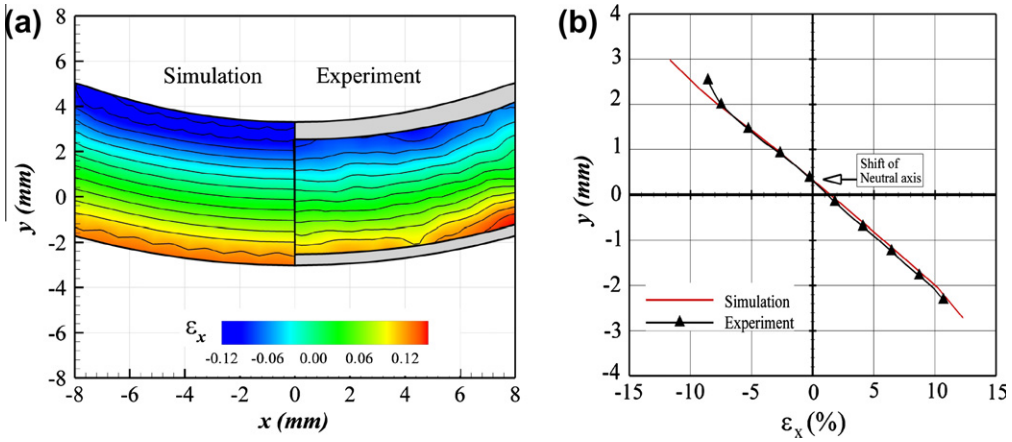


Fig. 13. Case 1 loading: (a) comparison of FE axial strain contours ($\varepsilon_x$) obtained with the proposed model against experimental data: $x$ = rolling direction (RD), $y$ = transverse direction (TD). (b) Axial strains ($\varepsilon_x$) vs. height at centerline.

compared to the simulation results. The comparison between experiment and simulation for case 1 is shown in Fig. 14 (symbols indicate the calculated cross-sectional geometry). Note that there is very little deformation perpendicular to the loading direction because this is the direction parallel to the *c*-axis of most of the grains.

Fig. 15a shows the comparison of the respective strain contours for case 2 (see Fig. 4) while a plot of the axial strain vs. the height of the beam at the center of the beam is shown in Fig. 15b. Again, very good agreement between experimental data and simulated results is obtained. The comparison of final cross-sections of the beam in case 2 loading is shown in Fig. 16. Note that the model accurately predicts that in this case there is more deformation perpendicular to the loading direction than in the previous case 1, since in case 2 this direction is aligned with the softer TD direction.

Fig. 17a shows the comparison between experimental and simulated strain contours for case 3. Note the very good agreement between the experimental and simulation results; in particular the significant upward shift of the neutral axis is very well described by the model (see Fig. 17b) .

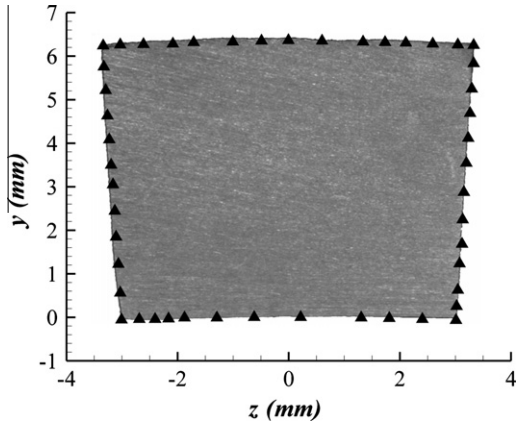


Fig. 14. Case 1: comparison of the photographed experimental cross-sections and FE simulation using the proposed model (symbols): $y$ = transverse direction (TD), $z$ = through-thickness direction (TT).

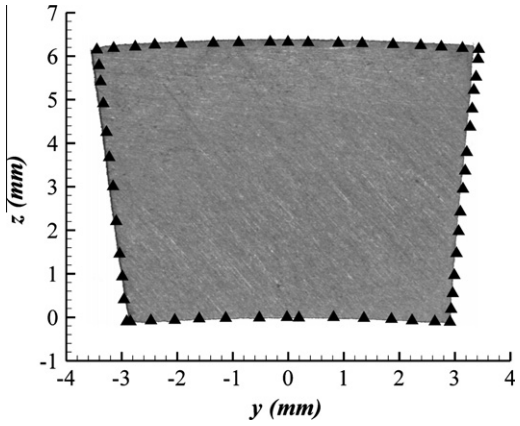


Fig. 16. Case 2: comparison of the photographed experimental cross-sections and FE simulation using the proposed model (symbols): $y$ = transverse direction (TD), $z$ = through thickness (TT).

The comparison between the photographed and simulated final cross-sections is shown in Fig. 18. The nearly square final cross-section as correctly predicted by the anisotropic model is a result of the hard to deform through-thickness direction being aligned normal to the loading direction in the cross-section.

Finally, Fig. 19a shows the comparison of the simulated and experimental axial strain contours in case 4, while Fig. 19b shows that in this case, once again, the model correctly predicts the shift of the neutral axis. Fig. 20 displays the comparison between predicted and measured cross-sections. Again, very good agreement was obtained.

## 5. Summary and concluding remarks

A set of experiments aimed at understanding the response of high-purity titanium at room temperature was reported in Ref. [12]. The cross-rolled plate investigated exhibits a strong basal texture. As a consequence, its mechanical response is non-symmetric (tension–compression asymmetry) and anisotropic. An elastoplastic orthotropic model that accounts for tension–compression

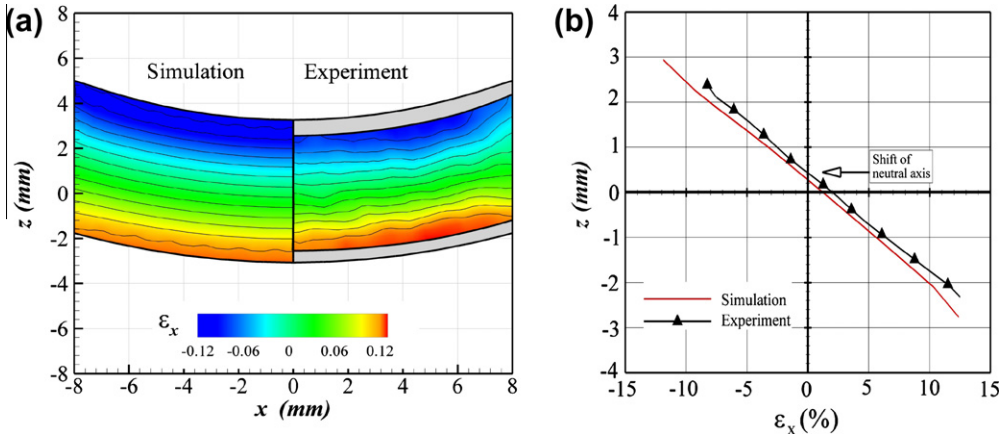


Fig. 15. Case 2 loading: (a) comparison of FE axial strain contours ($\varepsilon_x$), obtained with the proposed model and experimental data; (b) Axial strain ($\varepsilon_x$) vs. height at centerline. ($x$ = rolling direction (RD), $z$ = through thickness direction (TT).

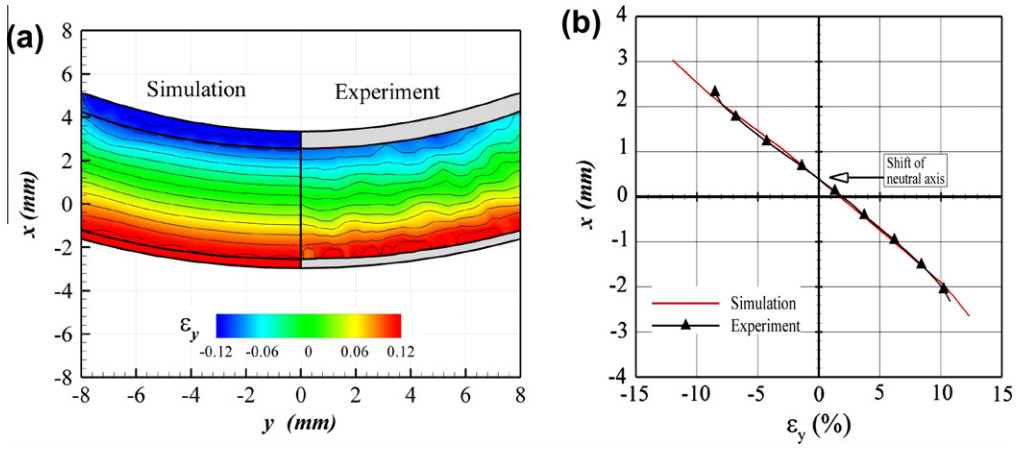


Fig. 17. Case 3 loading: (a) comparison of the FE axial strain contours ($\varepsilon_y$) obtained with the proposed model against experimental data. (b) Axial strains ($\varepsilon_y$) vs. height at centerline ($x$ = rolling direction (RD), $y$ = transverse direction (TD)).

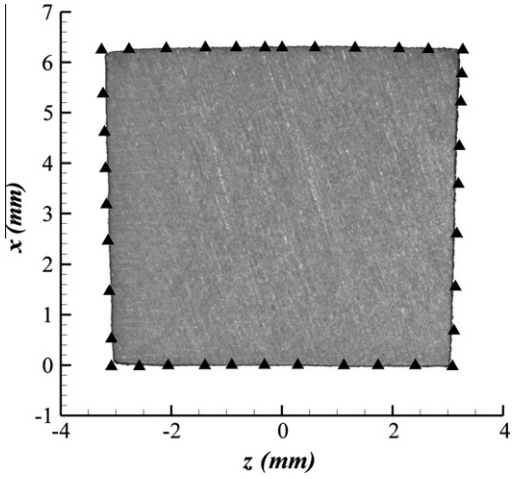


Fig. 18. Case 3: comparison of the photographed experimental cross-sections and FE simulation using the proposed model (symbols): $x$ = rolling direction (RD), $z$ = through-thickness direction (TT).

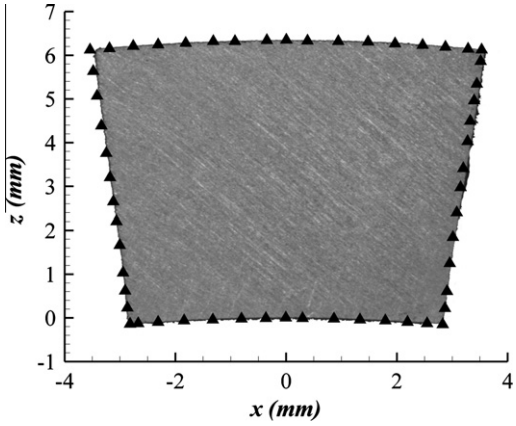


Fig. 20. Case 4: comparison of the photographed experimental and simulated (symbols) cross-sections: $x$ = rolling direction (RD), $z$ = through-thickness direction (TT).

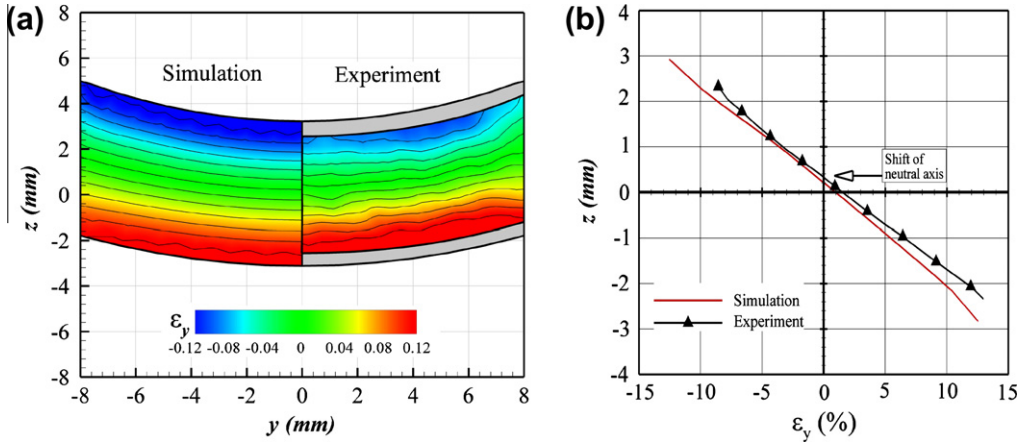


Fig. 19. Case 4 loading: (a) comparison of experimental and simulated axial strain contours ($\varepsilon_y$): $y$ = transverse direction (TD). (b) Axial strains ($\varepsilon_y$) vs. height at centerline $z$ = through-thickness direction (TT).

asymmetry was developed and described in Section 3. The ability of the developed model to capture the main features of the observed behavior of the high-purity titanium investigated was assessed by comparing the experimental data with simulation results in terms of stress–strain response in uniaxial tensile and compression tests in Ref. [12].

Here, we report the results of a series of bending experiments designed to validate the accuracy of the blue proposed description of the tension–compression asymmetry of the mechanical response of this material. The bent-beam geometry was selected for this high-purity α-titanium plate, and we expected to find qualitative differences between the response of the upper (top/compressive) and lower (bottom/tensile) fibers of the beam and a shift of the neutral axis, as a result of the directionality of twinning. The reason for this is that the uniaxial tension and compression tests had revealed that the tension–compression asymmetry of the material is highly directional. Thus, to further characterize the influence of this tension–compression asymmetry in bending loading, we conducted tests for different beam configurations and loading orientations with respect to the orthotropy axes. The deformed beams were analyzed using DIC to obtain the distribution of the local strain fields. The deformed cross-sections geometries were compared to the results of the corresponding simulations. The predicted strain fields and macroscopic shapes compare very well with experimental results. In addition, the upward shift of the neutral axis, which is due to the tension–compression asymmetry of the material, was particularly well described. This upward shift was most significant for case 3 loading because the tension–compression asymmetry of the material is most pronounced in the RD direction (see also a comparison between the experimental stress–strain curves in tension and compression shown in Fig. 18 of Ref. [12]).

The agreement between experiments and model predictions for all bending configurations is quite good. However, it should be acknowledged that the use of bending experiments only provides limited validation to the model. For an isotropic material response, the stress states that one explores with a bending test are uniaxial. On the other hand, as in the present case with texture-induced anisotropy, the stresses are indeed multiaxial, although with no significant amount of shear (i.e. with non-vanishing components only in the π-plane). To gain further understanding of the behavior of the material under a general stress state, an investigation of its behavior in simple shear needs to be performed. In addition, under simple shear loading it should be possible to achieve large homogeneous strains without any plastic instabilities such as necking in tension or barreling in compression. Such data will allow further validation of the model. Preliminary simple shear experiments on samples cut from the same titanium plate used in the present study have been reported elsewhere [1].

## References


[1] Ben Mhenini N, Gregori F, Bouvier S, Nixon M, Cazacu O. Simple shear response of high-purity alpha-titanium. In: Proceedings of the mecamat conference on nouvelles approches en mecanique experimentale, January 11–15, Aussois, France, in press.

[2] Cazacu O, Barlat F. A criterion for description of anisotropy and yield differential effects in pressure-insensitive metals. Int J Plast 2004;20:2027–45.

[3] Chun YB, Yu SL, Semiatin SL, Hwang SK. Effect of deformation twinning on microstructure and texture evolution during cold rolling of CP-titanium. Mater Sci Eng A 2005;398:209–19.

[4] Hill R. A theory of the yielding and plastic flow of anisotropic metals. Proc Roy Soc London A 1948;193:281–97.

[5] Hughes T. Numerical implementation of constitutive models: rate-independent deviatoric plasticity. In: Theoretical foundation for large scale computations for nonlinear material behavior, vol. 50; 1984. p. 2957.

[6] Kaschner GC, Bingert JF, Liu C, Lovato M, Maudlin PJ, Sout MG, et al. Mechanical response of zirconium II. Experimental and finite element analysis of bent beams. Acta Mater 2001;49:3097–108.

[7] Khan A, Kazmi R, Farroch B. Multiaxial and non-proportional loading responses, anisotropy and modeling of Ti–6Al–4V titanium alloy over wide ranges of strain rates and temperatures. Int J Plast 2007;23:931–50.

[8] Kim J, Ryou H, Kim D, Kim D, Lee W, Hong S-H, et al. Constitutive law for AZ31B Mg alloy sheets and finite element simulation for three-pointbending. Int J Mech Sci 2008;50:1510–8.

[9] Kuwabara T, Katami C, Kikuchi M, Shindo T, Ohwue T. Cup drawing of pure titanium sheet-finite element analysis and experimental validation. In: 7th international conference on numerical methods in industrial forming processes, 18–20 June, Toyohashi, Japan; 2001. p. 781–7.

[10] Lee D, Backofen WA. Yielding and plastic deformation in textured shett of titanium and its alloys. TMS–AIME 1966;236:1703–966.

[11] Li Q, Xu Y, Bassim MN. Dynamic mechanical behavior of pure titanium. J Mater Proc Technol 1997;155:1889–92.

[12] Nixon ME, Cazacu O, Lebensohn RA. Anisotropic response of high-purity α-titanium: experimental characterization and constitutive modeling. Int J Plast 2010;26:516–32.

[13] Plunkett B, Lebensohn RA, Cazacu O, Barlat F. Evolving yield function of hexagonal materials taking into account texture development and anisotropic hardening. Acta Mater 2006;54:4159–69.

[14] Salem AA, Kalidindi SR, Doherty RD. Strain hardening of titanium: role of deformation twinning. Acta Mater 2003;51:4225–37.

[15] Simo J, Taylor R. Consistent tangent operators for rate-independent elasto-plasticity. Comput Methods Appl Mech Eng 1985;48:101118.

[16] Sutton MA, McNeill SR, Helm JD, Chao YJ. Advances in two-dimensional and three-dimensional computer vision. Top Appl Phys 2000;77:323–72.